Silicon Nitride Building Blocks in the Visible Range of the Spectrum

Marçal Blasco-Solvas, Berta Fernández-Vior, Jad Sabek, Adrián Fernández-Gávela, Thalía Domínguez-Bucio, Frederic Y. Gardes, Carlos Domínguez-Horna, and Joaquín Faneca

***Abstract*—In this study, a platform guiding single-moded light at wavelengths of 480 nm, 520 nm and 633 nm (blue, green and red) is proposed and designed with several components being fabricated and characterised for the specific wavelength of 633 nm. A waveguide with propagation losses of 3.6 dB/cm is obtained, with a high confinement factor of 90.5% and a tight bending radius of 60 μm with 0.2 dB losses per bend, offering a good trade-off between losses, confinement factor and compactness. Also, a 1 $\times$ 2 MMI is demonstrated, with a footprint of 5 $\times$ 161 μm^2, and losses of 0.2 dB. Finally, a silicon nitride single-layer grating coupler has been validated to allow the fibre-to-chip coupling, with losses smaller than 11.7 dB. A comparison of the proposed platform with other state-of-the-art stoichiometric silicon nitride technologies performing in the range of the spectrum of 630–660 nm is shown. The present platform demonstrates losses in the order of the state-of-the-art single-mode waveguides, but with an enhancement of the confinement factor from 61% to 90.5%, which allows to decrease the bending radius by 20 μm or more compared with other state-of-the-art technologies.**

***Index Terms*—Silicon photonics, integrated photonics, visible spectrum, silicon nitride, building blocks.**

I. Introduction

In the last two decades, the market for photonic integrated circuits (PICs) has grown dramatically [1], [2], [3], [4], [5]. This growth has been mainly driven by telecommunication applications operating at 1550 nm and 1310 nm [6], [7], [8]. In this wavelength range, PICs use light to emit, detect, process, transmit and store information in order to overcome some of the major challenges faced by electronics today, particularly in terms of limited transmission speed, bandwidth and high power consumption [9]. Although the telecommunication band has been the most widely exploited, the visible range of the spectrum has broadened the possibilities to a whole new range of photonic applications including quantum computing [10], optogenetics [11], [12], biological sensing and spectroscopy [13], [14], imaging and display technologies [15], [16], [17], [18], light sources [19], [20], and underwater communication [21], amongst others [22], [23], [24]. Compared to free space optics, PICs offer miniaturisation, high reliability, energy efficiency and reduction in manufacturing and packaging costs.

Several material systems have been developed based on generic processes to offer stable and robust platforms for PICs, including silicon-on-insulator (SOI), indium phosphide, silicon dioxide (SiO_2) and silicon nitride (SiN) [25], [26], [27], [28], [29]. However, although many platforms are available, the bulk development of PICs and process design kits (PDKs) has focused on the SOI platform due to the low absorption losses it offers in the wavelength range between 1.1 μm and 3.7 μm. However, now that the wavelengths of interest have extended down to the visible part of the spectrum, SOI is no longer an option as guiding material, as it is not transparent at wavelengths below 1.1 μm. As a result, other material platforms have been explored for visible light applications, including the mature SiN platform, alumina (Al_2O_3) and aluminium nitride (AlN) [30].

Although SiN generally exhibits higher losses than Al_2O_3 [31], the CMOS compatibility and fabrication maturity of SiN makes it a promising material for further development for visible light integrated photonics platforms. In this case, CMOS compatibility indicates the standard fabrication process for semiconductor devices, in other words, it refers to the processes used in the semiconductor industry to fabricate integrated circuits. Since SiN is transparent throughout most of the visible range — down to at least 400 nm [32] — it is a viable candidate to implement "silicon photgonics" at wavelengths below 1.1 μm. SiN provides an alternative low-cost platform in which all fundamental non-active photonic components can be implemented. The advantages over Si are fabrication process flexibility, low temperature sensitivity, isotropic behaviour in all directions (amorphous material), refractive index and bandgap tuneability by varying the deposition conditions on the stoichiometry of the films, and higher transparency, which all enable the exploitation of SiN in the visible range. The versatility of the SiN platform

Manuscript received 8 April 2024; accepted 21 May 2024. Date of publication 23 May 2024; date of current version 2 September 2024. This work was supported in part by the Agencia Estatal de Investigación, MICIU/AEI/10.13039/501100011033 and for European Union NextGeneration EU/PRTR under Grant FJC2020-042823-I and Grant PLEC2022-009381, in part by U.K. Research and Innovation through Project "Silicon-rich silicon nitride Nonlinear Integrated Photonic ciRcuits Systems (juNIPeRS)" under Grant Nb EP/T007303/1 and "Rockley Photonics and the University of Southampton: A Prosperity Partnership" under Grant EP/R003076/1, in part by the H2020 EU Project Plasmoniac under Grant 871391, and in part by the Spanish Ministry of Science and Innovation (MICINN) through the MCI-21-PID2020-115204RB-I00 Project. *(Corresponding author: Joaquín Faneca.)*

Marçal Blasco-Solvas, Jad Sabek, Carlos Domínguez-Horna, and Joaquín Faneca are with the Instituto de Microelectrónica de Barcelona, IMB-CNM (CSIC), Campus UAB, 08193 Barcelona, Spain (e-mail: joaquin.faneca@imb-cnm.csic.es).

Berta Fernández-Vior and Adrián Fernández-Gávela are with the Physics Department, University of Oviedo, 33007 Oviedo, Spain.

Thalía Domínguez-Bucio and Frederic Y. Gardes are with the Optoelectronics Research Centre, University of Southampton, SO17 1BJ Southampton, U.K.

Color versions of one or more figures in this article are available at https://doi.org/10.1109/JLT.2024.3404639.

Digital Object Identifier 10.1109/JLT.2024.3404639

is key in the implementation of complex multi-layer photonic circuitry for photonic integrated applications in the range of the spectrum of 450–700 nm [33], [34].

A number of silicon nitride PIC foundries offer solutions with state-of-the-art PDKs at telecommunication wavelengths [35]. Having the SiN PIC technology already developed facilitates the opportunity to expand the PDK of SiN PICs to the visible range of the spectrum. In this sense, the development of individual building blocks to facilitate end users the possibility of designing and fabricating photonic integrated circuits in this range of the spectrum is key. The visible is a region of emerging interest for applications in integrated laser beam combiners, variable optical attenuators, interference pattern generators, bio-sensing, imaging and display, and more [36], together with the facilities in acquiring laser sources and photodetectors in this range. The different emerging applications that can exploit the PICs advantages lack from photonic standardisation of components, making more difficult the development of more complex systems in these areas. Various works have developed photonic integrated building blocks in the visible range of the spectrum [37], [38], [39], [40], [41], [42], [43], [44], [45], [46]. In all cases, the waveguide and device dimensions are smaller than in the near-infrared, especially in the blue-end of the spectrum, to maintain the single-mode or few-mode condition. The mode confinement in the waveguide is also higher at short wavelengths, which leads to higher sensitivity to surface roughness scattering and tighter fabrication tolerances. In this paper, the design of a unique single-mode waveguide geometry, that can support at the same time red (633 nm), green (520 nm) and blue (480 nm) is presented; and, specifically, silicon nitride building block components at 633 nm have been fabricated and characterised towards the first steps to develop a standarised SiN photonic integrated platform for the complete visible range.

II. Design and Fabrication

The platform used for operation in the visible wavelength regime consists of a 400 nm thick LPCVD SiN layer on a 3.2 μm buried oxide layer. The geometry of the waveguides in terms of slab thickness and width was optimised to satisfy single-mode propagation for TE polarisation at wavelengths of 480 nm, 520 nm and 633 nm at the same time, as can be seen in Fig. 1. Red and blue wavelengths have been chosen to cover the entire visible spectrum from 480 nm to 633 nm with the same waveguide geometry, satisfying the single-mode condition. Green has also been selected because is a really interesting regime for underwater communications [47], sensing [48], and imaging and display, controlling the use of red, green and blue (RGB) [49]. For the same SiN layer thickness, using rib waveguides allows to increase fabrication tolerances, avoiding working in the limiting regime of the Deep-UV lithography, while maintaining the single-mode condition at the three different wavelengths with the same structure. Rib waveguides soften the width requirements making the fabrication steps less strict in processes accuracy and present lower losses due to sidewall roughness [50]. This is why rib geometry was chosen over strip. As shown in the insert of Fig. 1(a), a waveguide width of 400 nm was selected to satisfy the single-mode condition for a slab thickness of 150 nm.

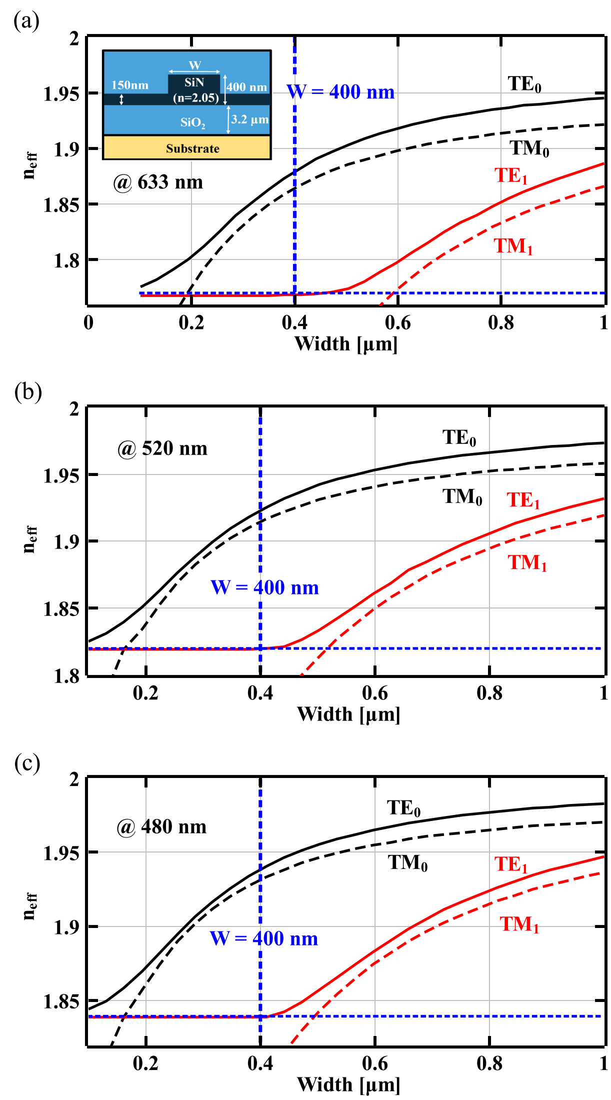

Fig. 1. Core width dependence of the effective index (n_{eff}) of LPCVD SiN waveguides with thickness of 400 nm and slab of 150 nm for wavelengths of (a) 633 nm, together with the cross-section schematic of the waveguide, (b) 520 nm, and (c) 480 nm.

In a similar manner, the bending radius of the waveguides was optimised by considering the contribution of the propagation losses (3.6 dB/cm), the radiative losses and the losses due to the mode mismatch between its straight and bent sections, assuming that the mode leakage towards the substrate was negligible. Fig. 2 shows that the optimal bending radius to reduce the total losses to values <0.05 dB/bend is 60 μm for the three different wavelengths, 480 nm, 520 nm and 633 nm.

There are different coupling methods from the optical fibre to chip. Even though the edge coupling can achieve lower losses and higher broadband than the grating couplers [51], the alignment tolerances are lower, apart from the required cleaving and polishing of the chips, ensuring that all the integrated waveguides maintain the same coupling interface [52]. Instead, grating couplers allow wafer scale testing without further fabrication steps or polishing treatments [53]. In order to couple light into the waveguides, grating couplers consisting of a 10 μm wide surface

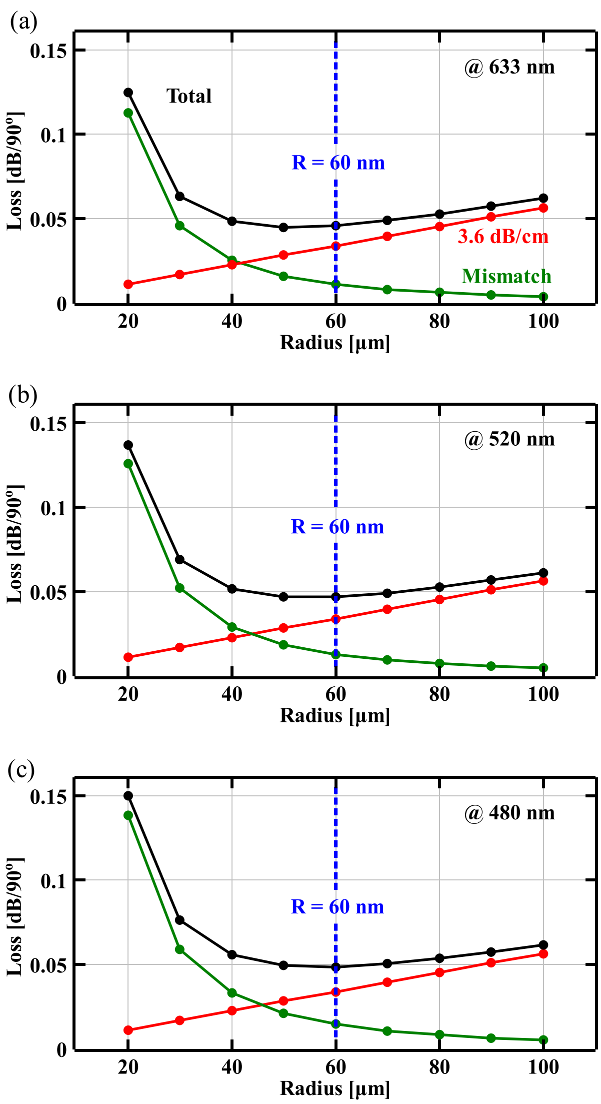

Fig. 2. Bend losses as a function of radius for the LPCVD SiN waveguides with a width of 400 nm for wavelengths of (a) 633 nm, (b) 520 nm, and (c) 480 nm.

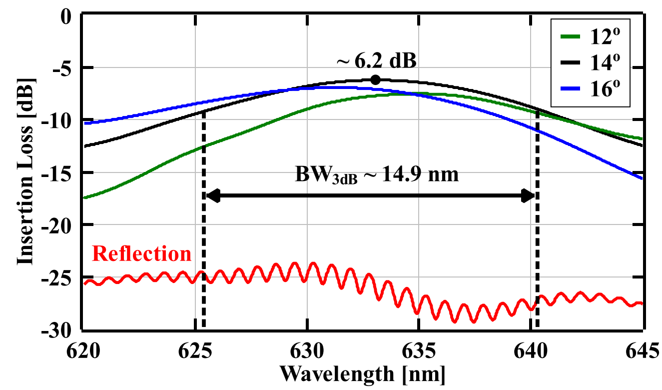

Fig. 3. Coupling efficiency (insertion loss) versus wavelength estimated for the grating coupler optimised at 633 nm with a coupling angle of 12°, 14° and 16°, period of 400 nm and filling factor of 50%.

grating were designed to have a sufficient coupling efficiency to characterise all the integrated optical components without the necessity of additional fabrication processes, one unique lithography and etching steps [38], [40]. These grating couplers were optimised to be efficient for TE polarisation, at a target wavelength of 633 nm and with a coupling angle of 14°. The designed and fabricated waveguides can support both TE and TM fundamental modes. However, the polarisation dependent components, such as grating couplers, and multi-mode interferometers (MMIs), have been selected to work for the TE mode. TE modes have lower group velocity compared with TM [54], which means that are less affected by material dispersion, making them more suitable for high-speed data transmission. The confinement factor of the TE mode is higher than the TM mode, being able to reduce the bending radius. Also, for TE mode, due to the confinement, the measured propagation losses are more associated to the core material than for the TM mode, reflecting the quality of the deposited SiN. The grating exhibited a theoretical coupling efficiency of 31.5% with a 3 dB bandwidth of 14.9 nm when using a period of 400 nm and filling factor of 50%, as illustrated in Fig. 3. The gratings were then tapered down to the single-mode width using an adiabatic taper with a length of 700 μm. Grating couplers designs for blue and green present limitations in terms of feature size, which are difficult to achieve by Deep-UV lithography. They can be done using e-beam lithography, however, it is a slow and expensive process, which is not practical for production.

Finally, 1 × 2 MMIs designed to evenly split light at wavelengths of 633 nm, 520 nm, and 480 nm, as depicted in Fig. 4(a), (b) and (c), have been implemented within PICs. These MMIs are preferred over directional couplers due to their superior tolerance to fabrication errors [55]. The width of the multi-mode region (W_{MMI}) was selected to be 5 μm to minimise the footprint of the device, while the length was set to 41 μm, 49 μm and 54 μm for wavelengths of 633 nm, 520 nm and 480 nm respectively, to achieve the desired splitting ratio (50:50) at the target wavelengths, as shown in Fig. 4(d), (e), (f). The width and the length of the input tapers were optimised to 2 μm and 60 μm respectively to provide the lowest optical loss possible. Several structures operating at 633 nm were included in the final layout to characterise the designed devices.

The devices were fabricated on 8 in (200 mm) Si wafers with a 3.2 μm thermally grown SiO_2 layer and a 400 nm LPCVD SiN layer. The structures were defined using a 680 nm M91Y photoresist and Deep-UV lithography. Then, they were transferred onto the SiN layer using inductively coupled plasma etching (ICP) with a SF6:C4F8 chemistry and a target etch depth of 250 nm. Finally, a 1 μm thick layer of PECVD SiO_2 was deposited on top of the devices at 350 °C. The devices were fabricated at University of Southampton.

III. Characterisation

In order to measure the optical losses of the designed SiN waveguides, several waveguides of different lengths, ranging from 2 mm up to 26 mm, have been fabricated. All of them have the same number of bends, which have a radius of 60 μm, and

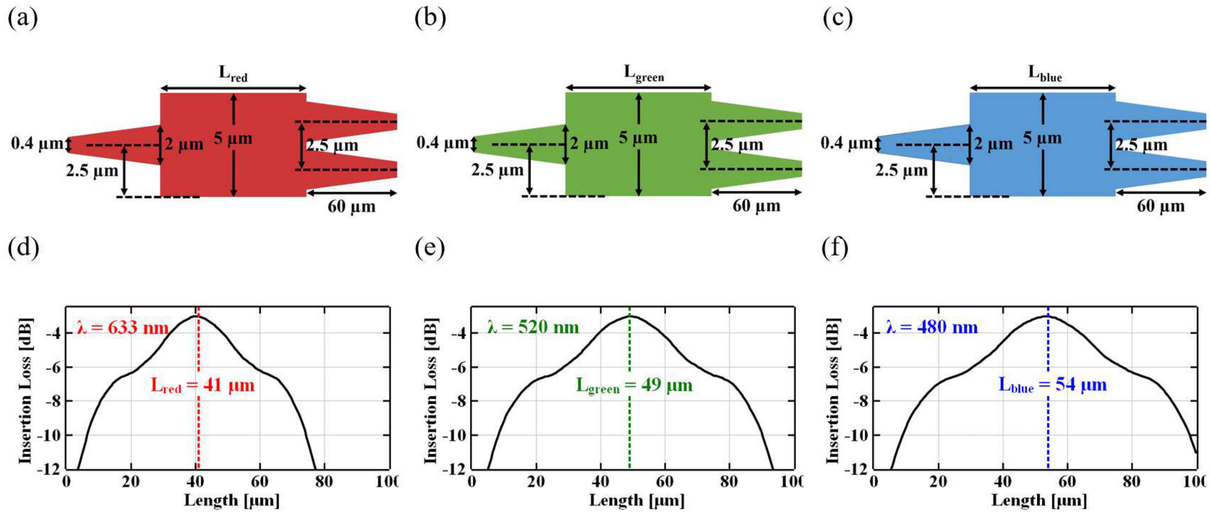

Fig. 4. Schematics of the designed MMIs for the different wavelengths (a) 633 nm, (b) 520 nm, and (c) 480 nm. Insertion loss against length at (d) 633 nm, (e) 520 nm, and (f) 480 nm.

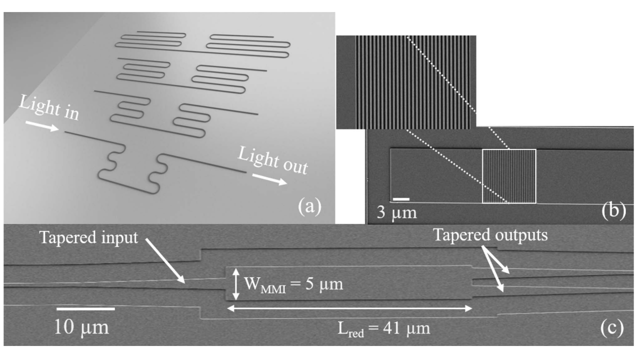

Fig. 5. (a) Waveguides schematic for different lengths and scanning electron microscope images of (b) a grating coupler and (c) MMI.

identical input and output grating couplers with tapers of 700 μm to match the single-mode waveguide width, as can be seen in Fig. 5(a). A Scanning Electron Microscope (SEM) was used to characterise the fabricated chips and to verify the dimensions of the three different components, which are all described in the design and fabrication section. The image of the grating couplers is depicted in Fig. 5(b), and their parameters can be observed, showing a period of 400 nm and a pitch of 200 nm, which are in line with the design parameters. The dimensions of the MMI are $W_{MMI} = 5\ \mu m$ and $L_{red} = 41\ \mu m$ with corresponding tapers of 60 μm narrowing down to a single-mode waveguide with a width of 400 nm, as shown in Fig. 5(c).

An in-house set-up was built in order to measure the propagation of the light along these components and their losses. In order to get a good, stabilised input signal, a He-Ne laser with an operating wavelength of 633 nm was used as laser source. As the light is coupled using grating couplers, it is necessary to control the position of the in-output fibre used for the light insertion. For that, the optical fibre was coupled to the laser source and the other side coupled to a polarisation controller to minimise the coupling losses. After the polarisation controller, the optical fibre is placed in a micro-manipulator stage with an angle controller. Also, the photonic chip was placed on top of a goniometer to ensure good alignment between the fibre and the grating coupler. Regarding the output signal, one side of an optical fibre was placed on an angle controller, positioned on another micro-manipulator stage, to ensure the right coupling angle, and the other side of the optical fibre was connected to a powermeter through a photo-diode sensor, where the output light intensity was measured. For inspection and easier manual alignment of the set-up, a camera was placed above the chip.

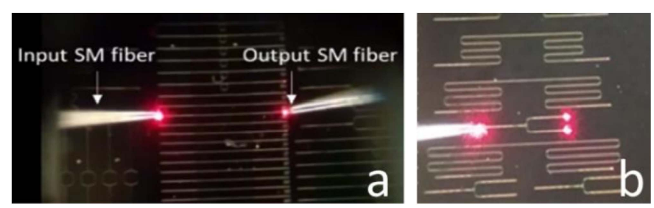

Fig. 6. Photonic characterisation images of the coupling between the optic fibre and the integrated components for (a) straight waveguides and (b) MMIs.

In Fig. 6(a), a microscope image demonstrates the input/output coupling of the 633 nm laser to a single-mode silicon nitride waveguide. The polarised light is injected by means of a single-mode optical fibre and coupling is performed through the designed grating coupler using an angle of $14^\circ \pm 2^\circ$. In Fig. 6(b) a microscope picture shows a SiN MMI splitter fed by a TE polarised laser at 633 nm.

IV. Results

Six different chips were fabricated and characterised. Each chip contains ten waveguides of different lengths, ranging from 7 mm to 28.33 mm as explained in the previous section, and three measurements for each waveguide were carried out. The mean value of these three measurements was taken as the value of the losses of each waveguide length for each chip. This process has been repeated for the six chips. The losses in the waveguides of different chips oscillate between 3 dB/cm up to 4.8 dB/cm

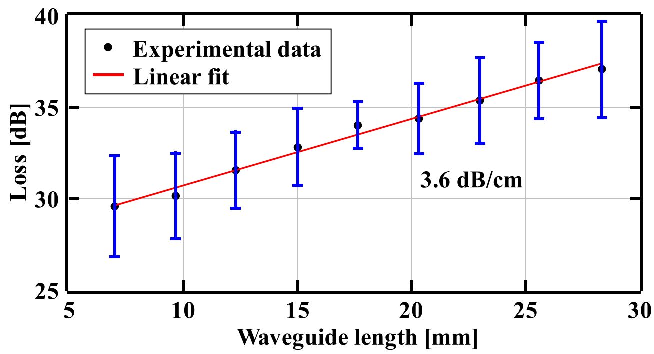

Fig. 7. Propagation loss for different waveguide lengths. The value shown is the mean of the measurements of six different chips. In blue, the corresponding error of each measurement.

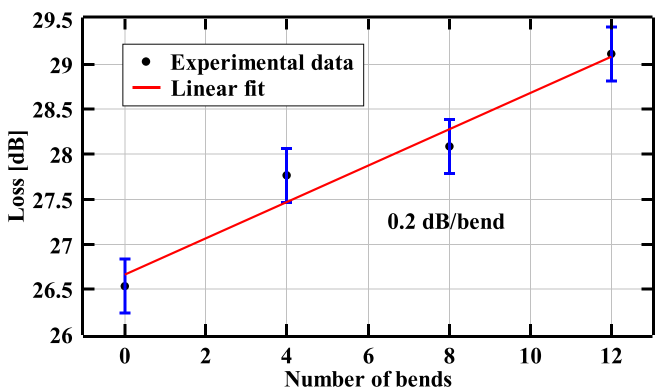

Fig. 8. Mean value loss for different number of bends with their corresponding error (in blue).

with a mean value of $3.6\,\mathrm{dB/cm}$. The mean value of all the measurements of every chip with its standard deviation is shown in Fig. 7.

From Fig. 7, the y-intercept was calculated, which has a mean value of $27.06\,\mathrm{dB}$. This value corresponds to the losses of sixteen bends (considering a single bend to be a 90° curvature with a radius of $60\,\mu\mathrm{m}$), two grating couplers, input and output, and two tapers of $700\,\mu\mathrm{m}$ length. In order to separate the bend loss contribution from the rest, a study of the losses in the bends was carried out for no bends and three different number of bends: four, eight and twelve. Like in the previous waveguide procedure, three measurements of each structure were carried out of six different chips, and their mean value was taken as the bend loss value. Fig. 8 shows the measurements of the structures with different number of bends. From there, a mean value of $0.2\,\mathrm{dB}$ per bend was experimentally demonstrated. It is worth mentioning that the losses per bending were expected to be 0.05 dB/bend according with simulations. This variance is caused by fabrication imperfections and sidewall roughness that were not present in the simulations and affect the bending losses. Multiplying these losses by the number of bends that are in the initially measured waveguides (16 bends), a total value of $3.2\,\mathrm{dB}$ is obtained as the contribution to the losses caused by the bends. Extracting this value, and the tapers loss ($0.5\,\mathrm{dB}$) to the $27.06\,\mathrm{dB}$ previously calculated in Fig. 7, a loss of $11.7\,\mathrm{dB}$

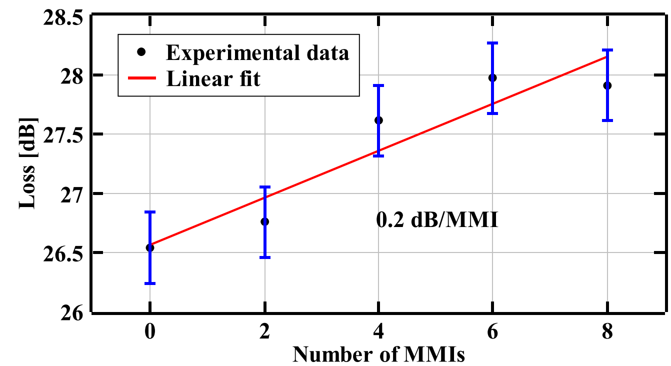

Fig. 9. Insertion loss for different number of MMIs with their corresponding error (in blue).

TABLE I
OPTICAL PERFORMANCE OF THE SIN BASIC BUILDING BLOCKS OPERATING AT 633 nm

Component	Losses
Waveguide	3.6 ± 0.2 dB/cm
Bend	0.20 ± 0.03 dB
Grating coupler	11.7 ± 0.6 dB
MMI	0.20 ± 0.04 dB

per grating coupler is obtained. The mentioned taper losses have been extracted from the waveguide propagation loss. The taper length of $700\,\mu\mathrm{m}$, times the waveguide loss $3.6\,\mathrm{dB/cm}$, results in $0.5\,\mathrm{dB}$, which are the highest losses this component will experience, as no losses from the adiabatic change are expected. In this loss, the value also contains the set-up loss, meaning: the loss of the connectors, the polarisation error, which produces ripples in the wavelength spectrum when is not $100\,\mathrm{percent}$ TE, the cleaving of the optic fibres facets and the error in the alignment angle ($\pm 2^\circ$), which is really sensitive [56], [57], as can be seen in Fig. 3. Apart from that, the fabrication tolerances and the box thickness can also affect the coupling efficiency [58]. Moreover, in the simulations, the mean value of the optical fibre mode field diameter, which is between 3.6-5.3 $\mu\mathrm{m}$ according with the fabricators, has been used. All these contributions are the reason of the difference between the simulated and experimental grating response.

Furthermore, in order to characterise the losses of the MMI building block, different number of MMIs were fabricated: two, four, six and eight. Again, three measurements for each structure were done and the mean value is selected for the plot, Fig. 9. From there, a loss of the MMI building block of 0.2 dB/MMI is demonstrated. Also, the ratio between the two outputs (P_1/P_2) was measured to be 1.015, which ensures a good splitting of light in half of the input signal. A summary of the results obtained for each individual component is shown in Table I.

In order to set side by side this study with the state-of-the-art stoichiometric SiN platforms performing in the range of the spectrum of 630–660 nm, Table II presents a comparison of reported SiN integrated technological characteristics. Technologies developed in ref. [43], [44] and [45] show multi-mode behavior and they all have a high confinement factor, with values of 91.3%, 69.1%, and 75.3% respectively; losses ranging from

TABLE II
STATE-OF-THE-ART STOICHIOMETRIC SiN PLATFORMS, OPERATING AT WAVELENGTHS BETWEEN 630 AND 660 nm

λ (nm)	Mode*	Width (nm)	Thickness (nm)	Cross-section (μm^2)	Confinement factor	Bend radius (μm)	Loss (dB/cm)
660 [43]	TE, MM	1000	320	0.32	0.913	400	1.71 ± 0.51
630 [44]	TE, MM	800	150	0.12	0.691	150	0.98
633 [45]	TE, MM	520	200	0.104	0.753	80	1.6 ± 0.7
640 [46]	TM, SM	1100	26	0.0286	0.048	7000	< 0.4
633 [45]	TE, SM	250	200	0.05	0.536	80	4.3 ± 0.7
633 [45]	TE, SM	290	200	0.058	0.610	80	3.7 ± 0.7
633 [This work]	TE, SM	400	400	0.16	0.905	60	3.6 ± 0.2

*TE: Transverse electric, TM: Transverse magnetic, SM: Single-mode, MM: Multi-mode.

$0.98\,\mathrm{dB/cm}$ up to $1.6\,\mathrm{dB/cm}$ and a bending radius from $80\,\mu\mathrm{m}$ up to $400\,\mu\mathrm{m}$. These propagation losses are 2.1–3.7 times lower than the ones of the platform presented in this paper, but the footprint is bigger, having bending radius as big as 1.2 to 6.7 times the radius of the studied technology. Other waveguides, like in the case of ref. [46], are single-moded and have losses smaller than $0.4\,\mathrm{dB/cm}$, which are 9 times lower than the losses of the presented waveguide geometry, but it shows a low confinement factor of 4.8%, which is 18.9 times lower than the confinement factor of the presented technology. This means that light travels mostly through the cladding layer in this platform, and the losses are more related to the losses of the cladding material rather than the losses of the core material. This fact implies a large bending radius of $7\,\mathrm{mm}$, which is 116.7 times larger than the one presented. Finally, reference [45] shows two single-mode platforms, which have similar losses compared with the present one, going from 3.7 to $4.3\,\mathrm{dB/cm}$, which are 1.2 and 1.03 times the losses of the studied components, respectively. They also have a similar bending radius of $80\,\mu\mathrm{m}$, which is 1.3 times larger than the presented radius. Finally, they have a smaller confinement of the light in its core material, 53.6% and 61.0% each, 0.59 and 0.67 times the confinement of the present study. The fact of having higher confinement factor allows lower dispersion in the operation wavelength range [59], [60], [61]. Comparing the technology of reference [45] with the presented in this study, both fabrications have been carried out using Deep-UV lithography. However, in this work, ICP etching has been chosen over RIE, one of the main differences in the fabrication process. The etching process has an impact in the propagation loss due to the sidewall roughness. Furthermore, the uniformity of the proposed SiN layer is 5%, reducing the variance in the fabricated waveguides propagation loss. The waveguide geometry and the quality of the deposited SiN material are also a factor that affect the losses.

In PICs, there is always a trade-off between losses and footprint [62]. Also, depending on the confinement factor, the losses can be more associated to the core material or to the cladding. With all that information, the studied technology arises with an equilibrium between a high confinement factor, optical losses and a low footprint. As mentioned previously, some of the compared platforms have low confinement, so the losses are more associated to the silicon oxide of the cladding material, where light is less absorbed and defects of the roughness are not that important, but they pay the price of having a larger bending radius. It must also be taken into account that the present technology operates at $633\,\mathrm{nm}$, which is equal to three other platforms and lower than the rest. Shorter wavelengths mean higher losses, as the optical extinction coefficient dispersion shows that the absorption of silicon nitride increases for shorter wavelengths. Apart from that, the studied platform demonstrated an input and output SiN single layer grating coupler without the presence of metal reflectors or multi-layer stack underneath. This is an important point, as a good coupling efficiency is obtained without complex fabrication processes, CMOS compatibility, and enabling the coupling between fibre and chip to be much easier than butt-coupling, increasing the alignment tolerances and allowing wafer-scale testing.

The waveguide cross-section has been chosen to satisfy the single mode condition at wavelengths of 480 nm, 520 nm and 633 nm at the same time, to avoid modal dispersion. Multi-mode integrated waveguides experience pulse spreading, due to the distinct paths that each of the modes follows [63]. In addition, having higher confinement factor, reducing the dispersion, can avoid the signals overlapping and interfering with each other, making easier for the receiver to process the information. Furthermore, optical communication systems that do not require dispersion-compensation schemes offer advantages in both the initial investment (lower transceiver price) and operation cost (lower power consumption), both key requirements for data transfer. These advantages can be exploited in applications such as visible light communications or Internet of Things, where sending information through the light is crucial. In the applications such as opto-genetics, biological sensing and spectroscopy, imaging and display technologies or underwater communications, the waveguide losses are not a big constrain, however having a high density of components is. Reducing the bending radius of the platform permits to increase the density of components that can fit in the same area for high volumes production. In quantum information, the visible spectrum is starting to play a big role because single-photon emitters in nitrogen rich silicon nitride have been demonstrated at room temperature [64]. However, the losses in quantum systems play a stronger role than the density of components, meaning that the presented cross-section will not be the ideal one for quantum applications, making the best candidate the platform in ref [46].

The presented technology shows passive components. Further studies may include the combination of functional materials with this platform, allowing active photonic building blocks, such as modulators, filters, switches or detectors. As SiN itself has no active capabilities, materials such as liquid crystals [65], phase change materials [66], [67], [68], thermal-heaters [69], graphene [70], [71] or transition metal dichalcogenides [72] could be used for adding the configurability to the passive devices.

V. Conclusion

In this work, SiN as core guiding material for the light propagation in the visible range of the spectrum, at a wavelength of 633 nm, is proposed. Basic photonic integrated circuit components such as single-mode waveguides, bends, grating couplers and MMIs have been designed, fabricated and characterised. All of them offering a competitive response comparable to the already existing cutting-edge platforms in the visible range. In future, this technology could be expanded with more passive building blocks, and different visible wavelengths such as green (520 nm) or blue (480 nm). The presented building blocks can be utilised in visible applications such as visible light communications, Internet of Things, bio-sensing, underwater communications or imaging and display, among others.

Acknowledgment

The authors would like to thank Bruno Santos for the measurements of the waveguides. Without the values provided by him, this work would not be fully completed.

References

[1] N. Margalit, C. Xiang, S. M. Bowers, A. Bjorlin, R. Blum, and J. E. Bowers, "Perspective on the future of silicon photonics and electronics," *Appl. Phys. Lett.*, vol. 118, no. 22, 2021, Art. no. 220501.
[2] D. Thomson et al., "Roadmap on silicon photonics," *J. Opt.*, vol. 18, no. 7, 2016, Art. no. 073003.
[3] Y. Li, Y. Zhang, L. Zhang, and A. W. Poon, "Silicon and hybrid silicon photonic devices for intra-datacenter applications: State of the art and perspectives," *Photon. Res.*, vol. 3, no. 5, pp. B10–B27, 2015.
[4] X. Chen et al., "The emergence of silicon photonics as a flexible technology platform," *Proc. IEEE*, vol. 106, no. 12, pp. 2101–2116, Dec. 2018.
[5] R. Soref, "The past, present, and future of silicon photonics," *IEEE J. Sel. Topics Quantum Electron.*, vol. 12, no. 6, pp. 1678–1687, Nov./Dec. 2006.
[6] B. Jalali and S. Fathpour, "Silicon photonics," *IEEE J. Lightw. Technol.*, vol. 24, no. 12, pp. 4600–4615, Dec. 2006.
[7] G. T. Reed, G. Mashanovich, F. Y. Gardes, and D. Thomson, "Silicon optical modulators," *Nature Photon.*, vol. 4, no. 8, pp. 518–526, 2010.
[8] B. J. Shastri et al. Prucnal, "Photonics for artificial intelligence and neuromorphic computing," *Nature Photon.*, vol. 15, no. 2, pp. 102–114, 2021.
[9] Y. Arakawa, T. Nakamura, Y. Urino, and T. Fujita, "Silicon photonics for next generation system integration platform," *IEEE Commun. Mag.*, vol. 51, no. 3, pp. 72–77, Mar. 2013.
[10] G. Moody et al., "2022 roadmap on integrated quantum photonics," *J. Phys.: Photon.*, vol. 4, no. 1, 2022, Art. no. 012501.
[11] R. Nazempour, Q. Zhang, C. Liu, and X. Sheng, "Design of silicon photonic structures for multi-site, multi-spectral optogenetics in the deep brain," *IEEE Photon. J.*, vol. 12, no. 6, Dec. 2020, Art. no. 4200107.
[12] L. Hoffman et al., "Low loss CMOS-compatible PECVD silicon nitride waveguides and grating couplers for blue light optogenetic applications," *IEEE Photon. J.*, vol. 8, no. 5, Oct. 2016, Art. no. 2701211.
[13] E. Luan, H. Shoman, D. M. Ratner, K. C. Cheung, and L. Chrostowski, "Silicon photonic biosensors using label-free detection," *Sensors*, vol. 18, no. 10, 2018, Art. no. 3519.
[14] P. Steglich, G. Lecci, and A. Mai, "Surface plasmon resonance (SPR) spectroscopy and photonic integrated circuit (PIC) biosensors: A comparative review," *Sensors*, vol. 22, no. 8, 2022, Art. no. 2901.
[15] C. V. Poulton et al., "Large-scale silicon nitride nanophotonic phased arrays at infrared and visible wavelengths," *Opt. Lett.*, vol. 42, no. 1, pp. 21–24, 2017.
[16] M. Raval, A. Yaacobi, and M. R. Watts, "Integrated visible light phased array system for autostereoscopic image projection," *Opt. Lett.*, vol. 43, no. 15, pp. 3678–3681, 2018.
[17] M. C. Shin et al., "Chip-scale blue light phased array," *Opt. Lett.*, vol. 45, no. 7, pp. 1934–1937, 2020.
[18] J. Notaros, M. Raval, M. Notaros, and M. R. Watts, "Integrated-phased-array-based visible-light near-eye holographic projector," in *Proc. IEEE Conf. Lasers Electro- Opt.*, 2019, pp. 1–2.
[19] M. Barth, J. Kouba, J. Stingl, B. Löchel, and O. Benson, "Modification of visible spontaneous emission with silicon nitride photonic crystal nanocavities," *Opt. Exp.*, vol. 15, no. 25, pp. 17231–17240, 2007.
[20] N. Chauhan et al., "Visible light photonic integrated Brillouin laser," *Nature Commun.*, vol. 12, no. 1, pp. 1–8, 2021.
[21] C. Shen et al., "20-meter underwater wireless optical communication link with 1.5 Gbps data rate," *Opt. Exp.*, vol. 24, no. 22, pp. 25502–25509, 2016.
[22] M. A. Porcel et al., "Silicon nitride photonic integration for visible light applications," *Opt. Laser Technol.*, vol. 112, pp. 299–306, 2019.
[23] F. Prieto et al., "An integrated optical interferometric nanodevice based on silicon technology for biosensor applications," *Nanotechnol.*, vol. 14, no. 8, 2003, Art. no. 907.
[24] C. Ranacher et al., "Characterization of evanescent field gas sensor structures based on silicon photonics," *IEEE Photon. J.*, vol. 10, no. 5, Oct. 2018, Art. no. 2700614.
[25] S. Y. Siew et al., "Review of silicon photonics technology and platform development," *IEEE J. Lightw. Technol.*, vol. 39, no. 13, pp. 4374–4389, Jul. 2021.
[26] T. Hu et al., "Silicon photonic platforms for mid-infrared applications," *Photon. Res.*, vol. 5, no. 5, pp. 417–430, 2017.
[27] P. Muñoz et al., "Silicon nitride photonic integration platforms for visible, near-infrared and mid-infrared applications," *Sensors*, vol. 17, no. 9, 2017, Art. no. 2088.
[28] A. Rahim et al., "Open-access silicon photonics platforms in Europe," *IEEE J. Sel. Topics Quantum Electron.*, vol. 25, no. 5, Sep./Oct. 2019, Art. no. 8200818.
[29] X. Leijtens, "Jeppix: The platform for indium phosphide-based photonics," *IET Optoelectron.*, vol. 5, no. 5, 2011, Art. no. 202.
[30] D. J. Blumenthal, "Photonic integration for UV to IR applications," *APL Photon.*, vol. 5, no. 2, 2020, Art. no. 020903.
[31] G. N. West et al., "Low-loss integrated photonics for the blue and ultraviolet regime," *Apl Photon.*, vol. 4, no. 2, 2019, Art. no. 026101.
[32] L. Y. Beliaev, E. Shkondin, A. V. Lavrinenko, and O. Takayama, "Optical, structural and composition properties of silicon nitride films deposited by reactive radio-frequency sputtering, low pressure and plasma-enhanced chemical vapor deposition," *Thin Solid Films*, vol. 763, 2022, Art. no. 139568.
[33] T. D. Bucio et al., "Silicon nitride photonics for the near-infrared," *IEEE J. Sel. Topics Quantum Electron.*, vol. 26, no. 2, 2019, Art. no. 8200613.
[34] F. Gardes et al., "A review of capabilities and scope for hybrid integration offered by silicon-nitride-based photonic integrated circuits," *Sensors*, vol. 22, no. 11, 2022, Art. no. 4227.
[35] C. G. Littlejohns et al., "Cornerstone's silicon photonics rapid prototyping platforms: Current status and future outlook," *Appl. Sci.*, vol. 10, no. 22, 2020, Art. no. 8201.
[36] D. Geuzebroek, R. Dekker, E. Klein, and J. van Kerkhof, "Photonic integrated circuits for visible light and near infrared: Controlling transport and properties of light," *Sensors Actuators B: Chem.*, vol. 223, pp. 952–956, 2016.
[37] A. Z. Subramanian et al., "Low-loss singlemode PECVD silicon nitride photonic wire waveguides for 532–900 nm wavelength window fabricated within a CMOS pilot line," *IEEE Photon. J.*, vol. 5, no. 6, Dec. 2013, Art. no. 2202809.
[38] S. Romero-García, F. Merget, F. Zhong, H. Finkelstein, and J. Witzens, "Visible wavelength silicon nitride focusing grating coupler with alcu/tin reflector," *Opt. Lett.*, vol. 38, no. 14, pp. 2521–2523, 2013.
[39] J. A. Smith, J. Monroy-Ruz, P. Jiang, J. G. Rarity, and K. C. Balram, "Toward compact high-efficiency grating couplers for visible wavelength photonics," *Opt. Lett.*, vol. 47, no. 15, pp. 3868–3871, 2022.
[40] J. H. Song et al., "Grating devices on a silicon nitride technology platform for visible light applications," *OSA Continuum*, vol. 2, no. 4, pp. 1155–1165, 2019.
[41] S. Romero-García, F. Merget, F. Zhong, H. Finkelstein, and J. Witzens, "Silicon nitride CMOS-compatible platform for integrated photonics applications at visible wavelengths," *Opt. Exp.*, vol. 21, no. 12, pp. 14036–14046, 2013.
[42] C. Sorace-Agaskar et al., "Versatile silicon nitride and alumina integrated photonic platforms for the ultraviolet to short-wave infrared," *IEEE J. Sel. Topics Quantum Electron.*, vol. 25, no. 5, Sep./Oct. 2019, Art. no. 8201515.
[43] M. Lelit et al., "Passive photonic integrated circuits elements fabricated on a silicon nitride platform," *Materials*, vol. 15, no. 4, 2022, Art. no. 1398.

[44] J. A. Smith, H. Francis, G. Navickaite, and M. J. Strain, "Sin foundry platform for high performance visible light integrated photonics," *Opt. Mater. Exp.*, vol. 13, no. 2, 2023, Art. no. 458.

[45] W. D. Sacher . et al., "Visible-light silicon nitride waveguide devices and implantable neurophotonic probes on thinned 200 mm silicon wafers," *Opt. Exp.*, vol. 27, no. 26, pp. 37400–37418, 2019.

[46] A. T. Mashayekh et al., "Silicon nitride pic-based multi-color laser engines for life science applications," *Opt. Exp.*, vol. 29, no. 6, pp. 8635–8653, 2021.

[47] G. Giuliano, S. Viola, S. Watson, L. Laycock, D. Rowe, and A. E. Kelly, "Laser based underwater communication systems," in *Proc. IEEE 18th Int. Conf. Transparent Opt. Netw.*, 2016, pp. 1–4.

[48] A. Zuniga, H. Flores, and P. Nurmi, "Ripe or rotten? Low-cost produce quality estimation using reflective green light sensing," *IEEE Pervasive Comput.*, vol. 20, no. 3, pp. 60–67, Jul.–Sep. 2021.

[49] F. Ponce and D. Bour, "Nitride-based semiconductors for blue and green light-emitting devices," *Nature*, vol. 386, no. 6623, pp. 351–359, 1997.

[50] S. M. Lindecrantz and O. G. Hellesø, "Estimation of propagation losses for narrow strip and rib waveguides," *IEEE Photon. Technol. Lett.*, vol. 26, no. 18, pp. 1836–1839, Sep. 2014.

[51] X. Mu, S. Wu, L. Cheng, and H. Fu, "Edge couplers in silicon photonic integrated circuits: A review," *Appl. Sci.*, vol. 10, no. 4, 2020, Art. no. 1538.

[52] L. Cheng, S. Mao, Z. Li, Y. Han, and H. Fu, "Grating couplers on silicon photonics: Design principles, emerging trends and practical issues," *Micromachines*, vol. 11, no. 7, 2020, Art. no. 666.

[53] Y. Lin et al.., "Low-loss broadband bi-layer edge couplers for visible light," *Opt. Exp.*, vol. 29, no. 21, pp. 34565–34576, 2021.

[54] E. Dulkeith, F. Xia, L. Schares, W. M. Green, and Y. A. Vlasov, "Group index and group velocity dispersion in silicon-on-insulator photonic wires," *Opt. Exp.*, vol. 14, no. 9, pp. 3853–3863, 2006.

[55] M. Rajarajan, B. M. A. Rahman, and K. T. V. Grattan, "A rigorous comparison of the performance of directional couplers with multimode interference devices," *IEEE J. Lightw. Technol.*, vol. 17, no. 2, pp. 243–248, 1999.

[56] Y. Ding, C. Peucheret, H. Ou, and K. Yvind, "Fully etched apodized grating coupler on the SOI platform with- 0.58 dB coupling efficiency," *Opt. Lett.*, vol. 39, no. 18, pp. 5348–5350, 2014.

[57] V. Vitali et al., "High-efficiency reflector-less dual-level silicon photonic grating coupler," *Photon. Res.*, vol. 11, no. 7, pp. 1275–1283, 2023.

[58] L. Vivien et al., "Light injection in SOI microwaveguides using high-efficiency grating couplers," *IEEE J. Lightw. Technol.*, vol. 24, no. 10, pp. 3810–3815, Oct. 2006.

[59] C. Xiang, W. Jin, and J. E. Bowers, "Silicon nitride passive and active photonic integrated circuits: Trends and prospects," *Photon. Res.*, vol. 10, no. 6, pp. A82–A96, 2022.

[60] A. Ayan, J. Liu, T. J. Kippenberg, and C.-S. Brès, "Towards efficient broadband parametric conversion in ultra-long SI 3 n 4 waveguides," *Opt. Exp.*, vol. 31, no. 24, pp. 40916–40927, 2023.

[61] J. K. Poon et al., "Silicon photonics for the visible and near-infrared spectrum," *Adv. Opt. Photon.*, vol. 16, no. 1, pp. 1–59, 2024.

[62] D. J. Blumenthal, R. Heideman, D. Geuzebroek, A. Leinse, and C. Roeloffzen, "Silicon nitride in silicon photonics," *Proc. IEEE*, vol. 106, no. 12, pp. 2209–2231, Dec. 2018.

[63] C. Li, D. Liu, and D. Dai, "Multimode silicon photonics," *Nanophotonics*, vol. 8, no. 2, pp. 227–247, 2018.

[64] A. Senichev et al., "Room-temperature single-photon emitters in silicon nitride," *Sci. Adv.*, vol. 7, no. 50, 2021, Art. no. eabj0627.

[65] J. Faneca, T. S. Perova, V. Tolmachev, and A. Baldycheva, "One-dimensional multi-channel photonic crystal resonators based on silicon-on-insulator with high quality factor," *Front. Phys.*, vol. 6, 2018, Art. no. 33.

[66] E. Gemo et al., "A plasmonically enhanced route to faster and more energy-efficient phase-change integrated photonic memory and computing devices," *J. Appl. Phys.*, vol. 129, no. 11, 2021, Art. no. 110902.

[67] J. Faneca et al., "On-chip sub-wavelength Bragg grating design based on novel low loss phase-change materials," *Opt. Exp.*, vol. 28, no. 11, pp. 16394–16406, 2020.

[68] J. Faneca et al., "Towards low loss non-volatile phase change materials in mid index waveguides," *Neuromorphic Comput. Eng.*, vol. 1, no. 1, 2021, Art. no. 014004.

[69] Z. Yong et al., "Power-efficient silicon nitride thermo-optic phase shifters for visible light," *Opt. Exp.*, vol. 30, no. 5, pp. 7225–7237, 2022.

[70] J. Faneca, B. T. Hogan, I. R. Diez, F. Y. Gardes, and A. Baldycheva, "Tuning silicon-rich nitride microring resonances with graphene capacitors for high-performance computing applications," *Opt. Exp.*, vol. 27, no. 24, pp. 35129–35140, 2019.

[71] J. Faneca, S. Meyer, F. Gardes, and D. N. Chigrin, "Graphene microheater for phase change chalcogenides based integrated photonic components," *Opt. Mater. Exp.*, vol. 12, no. 5, pp. 1991–2002, 2022.

[72] A. Singh, S. S. Jo, Y. Li, C. Wu, M. Li, and R. Jaramillo, "Refractive uses of layered and two-dimensional materials for integrated photonics," *ACS Photon.*, vol. 7, no. 12, pp. 3270–3285, 2020.

Marçal Blasco-Solvas received the B.S. degree in nanoscience and nanotechnology from the Universitat Autònoma de Barcelona, Barcelona, Spain, in 2021, and the M.Sc. degree in photonics from the Universitat Politècnica de Catalunya, Barcelona, in 2022. In 2023, he joined as a Ph.D. Student with the IMB-CNM, Barcelona, where he is currently involved in the developement of silicon nitride platforms for photonic integrated circuits in the visible range of the spectrum. His research focuses on PICs applications, such as photonic circuits for biosensors or holography.

Berta Fernández-Vior received the bachelor's degree in physics from the University of Oviedo, Oviedo, Spain, in 2023. During her last academic year, in 2022/23, she initiated the B.S. Final Project in the field of photonics, with a particular focus on the characterization of optical waveguides.

Jad Sabek received the degree in chemical sciences from the Abdelmalek Essaadi University of Tetuán, Tetouan, Morocco, in 2006, the master's degree in advanced studies in chemistry from the University of Seville, Seville, Spain, in 2007, the second master's degree in nanosciences and nanotechnology in 2014 from the Rovira i Virgili University of Tarragona, Tarragona, Spain, where he was involved in a European Research Project for the development of integrated wearable sensors for environmental and healthcare applications, and the Ph.D. degree in photonic integrated circuits based on silicon for the detection of cardiac biomarkers from Nanophotonic Technology Centre, the Polytechnic University of Valencia, Valencia, Spain, in 2019. He received a scholarship from the European Project, PHOCNOSIS, to carry out the Ph.D. degree. During that period, he has been involved in the design, fabrication, functionalization, and chemical and photonic characterisation of the devices. In 2020, he joined the IMB-CNM, Barcelona, Spain, participating in several projects, such as ConVaT, for the development of photonic sensors for the detection of covid19. He is a Member of the Photonic Platform for the development of photonic circuits located at the IMB-CNM. Moreover, he is Incharge platform visibility and responsible for communication within the Technological Hub of the Quantum technological Platform of CSIC. He has given several talks and presentations at different international and national conferences.

Adrián Fernández-Gávela received the B.S., M.S., and Ph.D. degrees in physics from the University of Oviedo, Oviedo, Spain, in 2008, 2009, and 2014, respectively. In 2014, he was a Postdoctoral Researcher with NanoBiosensors and Bioanalysis Applications Group,the Catalan Institute of Nanoscience and Nanotechnology, Barcelona, Spain. He was involved in many projects focused on optical biosensors applications. He was working in the design, fabrication, and characterisation of optical waveguide for bio-sensing. He was designing and fabricating microfluidic system for their integration in photonic chips. In 2016, he returned to the University of Oviedo, as an Assistant Professor and kept working in the discipline of optical biosensors, more specifically in the field of optical waveguide applications. Since 2021, he has been an Associate Professor with the University of Oviedo, keeping the same research field of interest.

Thalía Domínguez-Bucio received the B.S. degree in electronic and computer engineering from the Monterrey Institute of Technology, Monterrey, Mexico, in 2012, the M.Sc. degree in photonic technologies from the University of Southampton, Southampton, U.K., in 2013, and the Ph.D. degree for her thesis titled "NH_3-free PECVD Silicon Nitride for Photonic Applications" from Optoelectronics Research Centre (ORC), Southampton. She is currently a Senior Research Fellow in silicon photonics with ORC. Her research interests include the development of new material platforms, particularly silicon nitride, for novel emerging photonic applications.

Frederic Y. Gardes is currently a Professor with Optoelectronic Research Centre, the University of Southampton, Southampton, U.K. His most recent work is focusing on monolithic integration of Ge based quantum well devices and III/V devices with silicon nitride. He has authored or coauthored more than 250 publications in the field of silicon photonics and has multiple patents. His research interests include CMOS photonics and in particular high-speed active optical devices in silicon, germanium, and mid index waveguide.

Carlos Domínguez-Horna received the B.S., M.S., and Ph.D. degrees in chemistry from the Universidad Complutense of Madrid, Madrid, Spain, in 1980, and 1985, respectively. He became a Member of scientific staff with the Instituto de Microelectronica de Barcelona (IMB-CNM, CSIC), Barcelona, Spain, in 1986. Since 2002, he has been a Research Professor. In 1992, he founded the Chemical Transducers Group within the institute, having today 28 researchers and technicians, and has been recognised as a Technological Transfer Center by the Catalan Government. He is Member of the Spanish Royal Society of Chemistry, the Committee of Optoelectronics and Integrated Optics of the Spanish Optical Society, the Crystal Growth Group as part of the IOCG (International Organization of Crystal Growth), Member of the International Committee of Ibersensor, and Vocal Board of the Spanish Society of Sensory Science. He is also a Member of the Association European Photonic Industry Consortium Technology Platform Photonics21, SECPhO Technology Cluster (Cluster of Southern Europe Photonics and Optics), and the Optical Society of America. He is involved in materials and process development for new transducers and sensors. He is working on the development of an integrated optical technology based on silicon and silicon compounds for (bio)-chemical sensors and broad-band telecommunications applications.

Joaquín Faneca received the B.Sc. degree in physics from Universidad de Sevilla, Seville, Spain, in 2015, and the M.Sc. degree in new photonic technologies from Universidad Complutense de Madrid, Madrid, Spain, in 2016, and the Ph.D. degree in photonic engineering from the University of Exeter, Exeter, U.K. and the University of Southampton, Southampton, U.K., in 2020. He was awarded with the research fellowship from EPSRC (U.K.) to pursue the Ph.D. research project in photonic integrated circuits between the University of Exeter and University of Southampton, co-funded by the Company Lumentum Operations LLC. He has been part of the Project Junipers after finishing the Ph.D. from the University of Southampton, where silicon nitride non-linear properties were studied on chip. In 2020, he joined IMB-CNM through the European Project - CoNVat and obtained a Juan de la Cierva Postdoctoral Fellowship in 2022 to study silicon nitride photonic properties in the visible range of the spectrum. He has been involved in the design, simulation, fabrication, and characterization of actively tuneable devices based on Silicon and Silicon Nitride photonic integrated components, combined with reconfigurable materials, such as phase change materials, liquid crystals and graphene, which has been used as key components for photonic systems. He has also being involved in the study of the silicon nitride opto-electronic properties. He has given five invited talks in international photonic conferences, such as International Conference on Information Optics and Photonics (CIOP), International Photonics Conference (IPC) or Symposium on Silicon Based Optoelectronics (ISSBO) apart of assisting to more than 24 international conferences presenting oral talks and posters. He is also reviewer for technical journals *Scientific Reports*, *Optics Express*, *Optical Materials Express*, and *Nanoscale Research Letters*. He is Member of Optical Society of America, International Society for Optical Engineering, and has been part of the technical committee in 2022 of IEEE photonics conference, in communications and devices section.